

Ultrafast Laser Pulse Generation by Mode Locking: MATLAB-Based Demonstrations

Alexei Goun and Ksenija D. Glusac*



Cite This: <https://doi.org/10.1021/acs.jchemed.2c00981>



Read Online

ACCESS |



Metrics & More



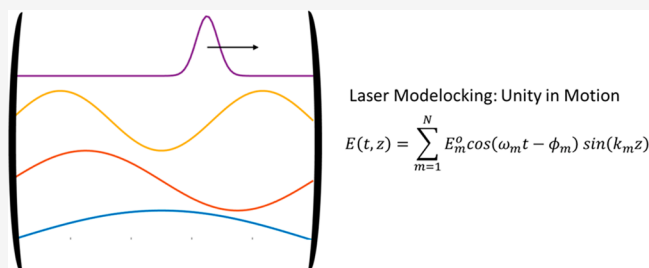
Article Recommendations



Supporting Information

ABSTRACT: Ultrafast laser spectroscopy is a valuable and increasingly accessible technique for studies of rapid chemical reactions. Critical to ultrafast spectroscopy is the concept of mode locking, a technique that enables a fixed phase relationship between laser modes, resulting in laser pulses with very short duration (in the fs or ps range). Despite the increasing importance of ultrafast lasers in chemistry, the introduction of key concepts behind their operation into the undergraduate and graduate chemistry coursework has been limited. To help the incorporation of these topics into chemistry courses, we report here a hands-on activity that helps students develop an intuitive understanding of the factors that impact electromagnetic wave evolution in optical cavities and the process of mode locking. We first provide the theoretical background by introducing cavity modes and contrasting them with well-known propagating electromagnetic waves. We then explore what happens when modes are added and how the relative phase between the modes affects their behavior. In the second section of this report, three teaching modules are provided, along with associated MATLAB codes and animated images, that can be used in the classroom to introduce concepts of cavity modes and mode locking. These teaching modules start by contrasting propagating electromagnetic waves with cavity modes and then illustrate what happens when multiple modes are present in the cavity and how the relative phase between the modes affects the overall electromagnetic field in the cavity.

KEYWORDS: Graduate, Undergraduate, Physical Chemistry, Ultrafast Lasers, Mode Locking



INTRODUCTION

Ultrafast laser spectroscopy is a valuable and increasingly accessible technique for studies of rapid chemical reactions.¹ The most commonly used ultrafast technique is pump–probe spectroscopy (also known as transient absorption spectroscopy), which allows one to monitor reaction kinetics on femtosecond time scales by initiating a chemical reaction using a pump laser pulse (usually in the UV/vis range) and studying reaction intermediates by probing their spectroscopic signatures in the UV/vis, IR, or microwave regions. For example, pump–probe spectroscopy has been essential for elucidation of the visual perception mechanisms in rhodopsins, where the visual perception was shown to begin with an ultrafast, vibrationally coherent cis–trans photoisomerization of a retinal chromophore taking place on femtosecond time scales.^{2,3} Pump–probe spectroscopy also provides structural information on molecular excited states, particularly when probed in the mid-IR region. For example, we showed that the changes in vibrational frequencies and the presence/absence of transient vibrational features report on the extent of electronic delocalization in metal-to-ligand charge transfer (MLCT) states of Re-based transition metal complexes.⁴ Even better structural information can be obtained by probing in the X-ray region, which provides element-specific information regarding

changes in the oxidation state or coordination environment of transition metal complexes in their excited states.⁵

In addition to providing a wider spectral window to probe reaction intermediates, the coherent extension of the spectral bandwidth from terahertz to the UV and even soft X-ray ranges has enabled significant shortening of the pulse duration. Pulses can now be significantly shorter than any intramolecular process, potentially allowing novel types of chemical reaction control, where a combination of laser pulses with varying phases and frequencies allows one to promote favorable reaction pathways in the chemical transformation.⁶ Short laser pulses are also used in the imaging of living tissue, where the high field strength of the femtosecond pulse easily induces the nonlinear response in the material.^{7,8} The high intensity of ultrafast lasers has also been applied in materials research. For example, nonlinear multiphoton initiation of photopolymerization is used in 3D lithography to generate complex structures

Received: October 3, 2022

Revised: January 1, 2023

with spatial accuracy down to half of the optical wavelength.⁹ Another interesting application of ultrafast pulses involves the creation of extreme states of matter such as shock waves¹⁰ or extreme magnetic fields.¹¹ The entire range of possibilities is still an active research area.

Critical to all of these novel applications is the development of mode-locked lasers. Mode locking is a technique that enables the introduction of a fixed phase relationship between different laser modes, resulting in laser pulses with very short duration (in the fs or ps range).¹² Several mode-locking techniques are used, which are commonly grouped into active and passive methods. For example, Kerr lens mode locking is a passive method that utilizes a nonlinear optical medium that changes its index of refraction as a function of applied electric field. When placed inside the laser cavity, this Kerr lens medium acts as an effective saturable absorber that allows the high intensity beam to pass while attenuating the weak wings of the pulse. Such preferable transmission of intense light leads to increasingly short pulses after each cavity round-trip before the steady state is achieved. Mode-locked lasers are applied not only in ultrafast laser spectroscopy but also in frequency comb spectroscopy,¹³ where the exact knowledge of the mode frequencies and the spacing between them allows for precision measurements needed for metrology, calibration of atomic spectrographs, attosecond pulse generation, and other applications.

Despite the increasing importance of ultrafast lasers in chemistry, the introduction of key concepts behind their operation into undergraduate and graduate chemistry coursework has been difficult. Chemistry students generally do not take optics and mathematics courses that are needed to introduce this topic efficiently. Consequently, cavity modes, mode locking, chirped pulse amplification, nonlinear optics, and other concepts important for the operation of ultrafast lasers are introduced only in occasional graduate-level spectroscopy books.^{14,15} To help the incorporation of these topics into undergraduate- and graduate-level chemistry courses, we report here a hands-on activity that provides students an intuitive understanding of the factors that impact electromagnetic wave evolution in optical cavities and the process of mode locking. In specific, we provide several MATLAB¹⁶ programs that are designed to illustrate how modes are formed within the laser cavity and how their frequency range, relative phases, and other parameters affect the mode-locking process. MATLAB was selected as a programming tool because it has been successfully utilized as a teaching tool in many chemistry-related demonstrations.¹⁷ For universities that do not have a software license, MATLAB codes can now be executed in the Python environment using MATLAB Compiler SDK,¹⁸ allowing code sharing with users, royalty-free.

BACKGROUND

While it is understood that light exhibits wave–particle duality, the description of cavity modes and mode locking can be readily achieved by considering only the wave behavior of light.¹⁵ We will start our discussion with the description of propagating waves. In specific, we will consider light as an electromagnetic (EM) plane wave propagating in the z direction. Outside the cavity, the solution to Maxwell's equations for the EM plane wave can be expressed as

$$\mathbf{E} = E_{\max} \cos(kz - \omega t + \phi) \hat{\mathbf{x}} \quad (1)$$

$$\mathbf{B} = B_{\max} \cos(kz - \omega t + \phi) \hat{\mathbf{y}} \quad (2)$$

where \mathbf{E} and \mathbf{B} are the electric and magnetic field vectors of the EM wave, E_{\max} and B_{\max} are the amplitudes of the electric and magnetic components, ω is the angular frequency of the wave ($\omega = 2\pi\nu$, where ν is the frequency), and k is the wavenumber ($k = 2\pi/\lambda$, where λ is the wavelength in vacuum). Vacuum conditions are considered here for simplicity, to focus on the essential properties of optical cavities and associated field modes. In real applications, light propagates in air, where dispersion (variation of the refractive index with the light wavelength) is expected to affect mode locking. While these effects are important when the propagation distance becomes large (such as in open-space atmospheric measurements), they will not be considered in this paper. The vectors $\hat{\mathbf{x}}$ and $\hat{\mathbf{y}}$ are the unit vectors associated with electric and magnetic fields, respectively. The plane-polarized light defined by eqs 1 and 2 has been arbitrarily chosen to propagate along the z direction and to have electric and magnetic field vectors along the x and y axes, respectively. To understand cavity modes, we will concentrate only on the electric field component of the EM wave. For this reason, our future discussion will describe the EM wave using the electric field component, whose magnitude can be expressed as a cosinusoidal function of z and t :

$$E(t, z) = E_{\max} \cos(kz - \omega t + \phi) \quad (3)$$

Equation 3 can be visualized as shown in Figure 1A, which plots E as a function of z for several selected time points. The

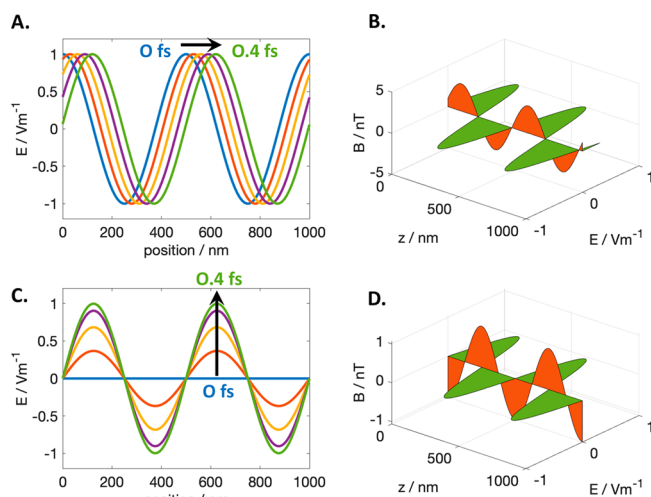


Figure 1. Comparison between (A, B) freely propagating waves and (C, D) plane waves inside a cavity. Panels (A) and (C) show how the electric field changes at four time intervals (0.0, 0.1, 0.2, 0.3, and 0.4 fs). Panels (B) and (D) show the relative phases of the electric and magnetic field components at a given time interval ($t = 2$ fs). Equation 3 was used for the plots in (A) (parameters: $E_{\max} = 1$ V/m, $\lambda = 500$ nm, $\phi = 0$), while eq 4 was used for the plots in (C) (parameters: $E_m^0 = 1$ V/m, $\lambda_m = 500$ nm, $L = 1$ μm , $\phi_m = \pi/2$). Equations 1 and 2 were used for the plot (B), while eqs 4 and 5 were used for the plot in (D) ($E_{\max} = 1$ V/m, $\lambda = 500$ nm, $\phi = 0$).

electric field vector points along the x direction, as defined by eq 1. We can see that the electric field intensity varies with position in a cosinusoidal fashion, while different time delays show that the wave propagates in the z direction.

The behavior of an EM plane wave changes drastically when it is placed between cavity mirrors. The plane wave will reflect

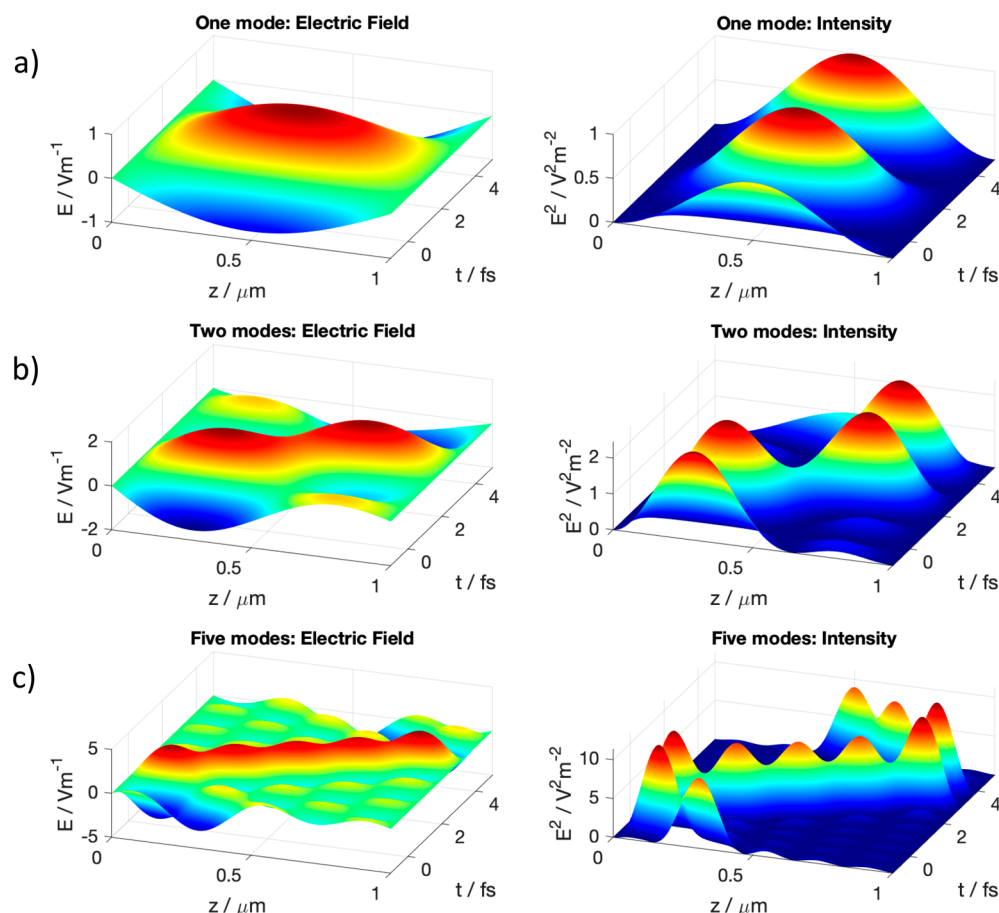


Figure 2. Mode locking: the graphs illustrate how the total electric field and intensity of light change as the number of modes in the cavity is increased from (a) 1 to (b) 2 to (c) 5. The simulations were made using eq 6 with the following parameters: E_m^0 for each mode was set to 1 V/m, ϕ_m for each mode was set to $\pi/2$, and the cavity size was set to $L = 1 \mu\text{m}$. The wavelength of each mode was set to be $2L/m$, where m is the mode number ($m = 1, 2, 3, 4, 5$).

from mirror surfaces, leading to interference between the propagating wave and its reflections. The interference may be destructive, leading to an overall magnitude loss. However, selected EM waves will undergo constructive interference, leading to the formation of standing waves. The conditions for constructive interference are dictated by the relationship between the wavelength of light (λ) and the length of the laser cavity (L). In specific, a standing wave will be formed if the ratio $2L/\lambda$ is an integer. Such a standing wave is called a cavity mode. When Maxwell's wave equations are solved under the standing wave conditions for the cavity formed by two perfectly conducting mirrors at $z = 0$ and $z = L$, the cavity mode with index m in one dimension can be described as

$$E_m(t, z) = E_m^0 \cos(\omega_m t - \phi_m) \sin(k_m z) \quad (4)$$

where E_m^0 is the amplitude, ϕ_m is the phase of the wave, and these parameters are defined as described in the Appendix 1. In our model, the electric field vector is selected to be along the x axis. The parameters ω_m and k_m are the angular frequency and the wavenumber of the mode, respectively, and their values are restricted to those that can be written as

$$k_m = \frac{m\pi}{L}$$

$$\omega_m = \frac{m\pi c}{L}$$

where m is an integer ($m = 1, 2, 3, \dots$). Equation 4 is visualized in Figure 1C, which plots the variation of E with position z at different time intervals. The most striking difference between the plots in Figure 1A and Figure 1C is that the former represents a propagating wave, while the later represents a standing wave. It is also important to mention that the $\lambda = 500 \text{ nm}$ and $L = 1 \mu\text{m}$ were selected in Figure 1B to match the standing wave condition ($2L/\lambda = \text{integer}$). If the plane wave inside the cavity does not satisfy the standing wave condition (for example, $\lambda = 501 \text{ nm}$ and $L = 1 \mu\text{m}$), destructive interference will occur between the wave and its reflection from the cavity mirrors, preventing a buildup of the electric field in the cavity.

Even though most of our discussion focuses on the electric field component of the electromagnetic radiation, it is interesting to comment on the role that the magnetic field plays in cavity modes. In the case of a propagating electromagnetic wave (eqs 1 and 2), the electric and magnetic fields oscillate with the same phase and reach maximum and minimum values at the same positions and times (Figure 1C). The situation is different in the case of cavity modes, where the magnetic field $B_m(t, z)$ is expressed as

$$B_m(t, z) = -\frac{E_m^0}{c} \sin(\omega_m t - \phi_m) \cos(k_m z) \quad (5)$$

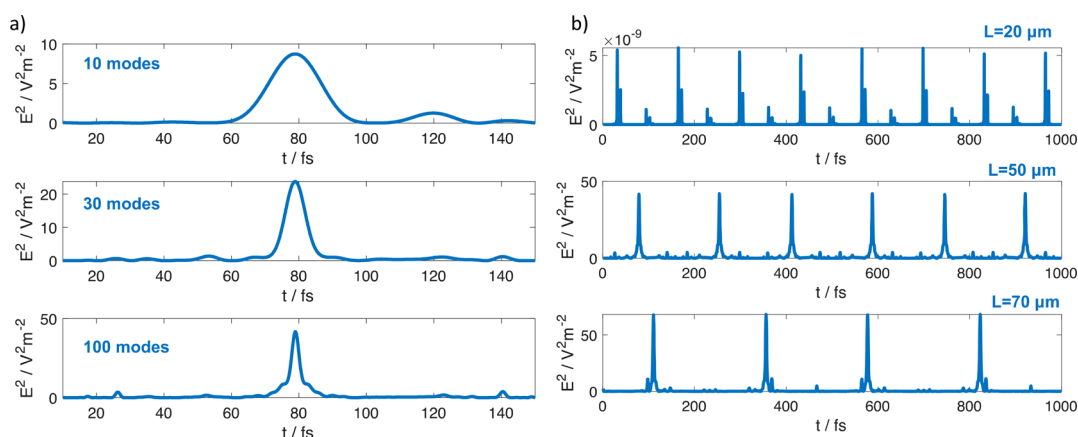


Figure 3. Temporal behavior of laser pulses. (a) Widths of pulses obtained using $N = 10, 30,$ and 100 modes. The simulations were obtained using eq 6 and the initial field $\frac{E(0,z)}{\text{V m}^{-1}} = \left(\frac{1}{\sqrt{2}} \right) \cdot \sin\left(\frac{2\pi(z-ct)/\mu\text{m}}{1.55 \cdot 10^{-6}/\mu\text{m}} \right) \cdot \exp\left[-\left(\frac{(z-ct-32 \cdot 10^{-6})/\mu\text{m}}{4 \cdot 10^{-6}/\mu\text{m}} \right)^2 \right]$. The cavity length was set to $L = 50 \mu\text{m}$. The wavelength of each mode was set to be $2L/m$, where m is the mode number ($m = 1, 2, 3, \dots$). Temporal data are plotted for $z = 23 \mu\text{m}$. (b) Repetition rates of pulses obtained for cavity sizes $L = 20, 50,$ and $70 \mu\text{m}$. The number of modes was set to $N = 100$. The initial field $E(0, z)$ and the wavelength of each mode were defined as described in (a).

Equation 5 is derived in Appendix 1, and the resulting wave is plotted in Figure 1D. In our model, the magnetic field vector is selected to be along the y axis. The relationship between the electric and magnetic fields of the cavity mode can be compared to the relationship between the kinetic and potential energies in the harmonic oscillator. Just as the kinetic and potential energies of the harmonic oscillator interchange their values as the oscillator is displaced from its equilibrium position, the electric and magnetic fields of the cavity mode exhibit similar displacement in time: when electric field is at its maximum, the magnetic field is at the minimum value. Since the overall energy density of the electromagnetic wave is obtained as a sum of electric and magnetic field components,

$$u = \frac{\epsilon_0}{2} E^2 + \frac{1}{2\mu_0} B^2$$

$$= \frac{\epsilon_0 (E_m^0)^2}{4} [1 - \cos(2(\omega_m t - \phi_m)) \cos(2k_m z)] \quad (6)$$

there is a persistent spatial redistribution of the electromagnetic energy within the cavity. The standing mode of the electromagnetic field in this respect is very similar to a standing mode of an elastic rope, where elastic energy stored in the nodes is transferred to kinetic energy of the antinodes. This redistribution is illustrated in Figure 1D and Supporting Video TM1b, which show the presence of spatial points within the cavity where the electric field strength is at a maximum while the magnetic field strength is zero and vice versa.

Next, we consider what happens when multiple modes with different frequencies are placed inside the cavity. The overall electric field is then expressed as the sum of N individual modes, while the intensity $I(t, z)$ is proportional to the square of the electric field:

$$E(t, z) = \sum_{m=1}^N E_m^0 \cos(\omega_m t - \phi_m) \sin(k_m z)$$

$$I(t, z) \propto E(t, z)^2 \quad (7)$$

Our simulations assume a linear regime of light–matter interactions, allowing superposition of the modes. Once the

peak optical power is beyond the linear response regime of the material, complex coupled mode interactions need to be analyzed. Figure 2 illustrates how the total electric field E and the corresponding intensity I change as the number of modes is changed from one to two to five. As the number of modes is increased, the standing wave converts into a propagating pulse. For example, when only one mode is present (Figure 2a), the pulse is centered at $0.5 \mu\text{m}$ and oscillates in intensity at this point without any motion along cavity's z axis. In contrast, the presence of five modes (Figure 2c) generates a pulse that is initially located at $\sim 0.1 \mu\text{m}$ and moves with time along the z axis. After 4 fs, the pulse is located at $\sim 0.8 \mu\text{m}$. This pulse propagation is essential for applications in ultrafast laser spectroscopy, as it enables the formation of pulses with variable time duration.

Importantly, the temporal width of the pulse is directly related to the number of modes: a higher number of modes leads to shorter pulses. Figure 3a shows that the pulse width becomes increasingly shorter as the number of modes N increases from 10 to 30 to 100. This behavior shows that the generation of ultrashort laser pulses requires a lasing medium with a broad emission range to enable enough modes for the generation of femtosecond pulses. This relationship between the number of modes and the pulse duration is another demonstration of the Heisenberg uncertainty principle, expressed as $\Delta E \Delta t \geq \hbar/2$. The large number of modes with different frequencies gives rise to a large uncertainty in energy (large ΔE), which in turn results in a small uncertainty in time (Δt) and short laser pulses. The intensity of each pulse is proportional to the square of the number of modes, showing that intense and short laser pulses are produced. The temporal spacing between pulses is controlled by the cavity length and can be calculated as $2L/c$.¹² As the length of the cavity increases, the spacing between the pulses increases, leading to lower repetition rate (number of pulses per second) of the laser (Figure 3b). For example, commercial Ti:sapphire oscillator lasers operate at a repetition rate of ~ 80 MHz, which corresponds to a cavity with length $L \sim 2$ m.

To enable the formation of such short pulses, it is essential that the phases of individual modes are fixed. For example,

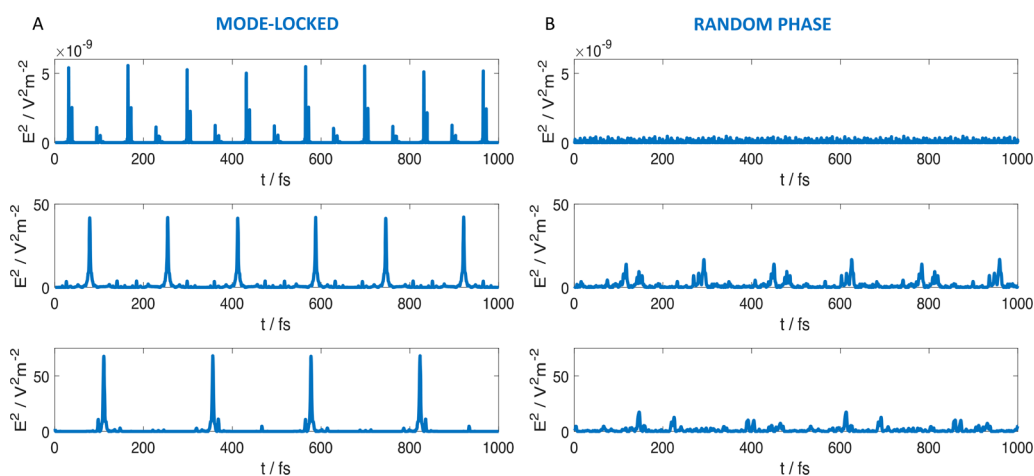


Figure 4. Effect of the phase on pulse generation. The simulation was made using the same parameters as in Figure 3B. The mode-locked graph was obtained by setting the phase of each mode as described in Figure 3B, while the random-phase graph was obtained by setting a random value ranging from 0 to 2π for each mode.

Table 1. Teaching Modules and Their Input/Output Parameters and Learning Objectives

Teaching Module Number	Teaching Module Title	Parameters to Change	Output	Learning Objectives
1	Animation: propagating versus standing EM waves	Input wavelength (for propagating wave) and mode index (for standing wave)	Animated graph showing how E and B change with time	<ol style="list-style-type: none"> 1. E and B vector directions 2. Time evolution: propagating versus standing waves 3. Relative E and B phases 4. Effect of wavelength on spatial and temporal dependence
2	Single versus multiple modes	Number of modes	Animated graphs showing distribution of electric fields and intensities	<ol style="list-style-type: none"> 1. Single mode is a standing wave in the cavity 2. Interference between two or more modes leads to the traveling pulse
3	Coherent versus random phases	Relative phase of modes Number of modes Cavity length	Graph of pulse train as a function of time	<ol style="list-style-type: none"> 1. Importance of maintaining a fixed phase relationship between modes 2. Scaling of the peak power of the mode-locked laser with the number of modes versus incoherent combination of those

when all modes oscillate with the same phase (for example, the phase of every mode was set to $\pi/2$ in Figure 4A), intense short pulses are formed. However, when the phases are set to be random, a fluctuating output is formed (Figure 4B). The process by which the cavity modes are placed into such a fixed phase relationship is called mode locking. This process is critical to the formation of ultrashort laser pulses, as illustrated in the Supporting Video TM2b. This video shows that the constructive and destructive interference between five individual modes with same phase leads to the generation of short and propagating pulses of light. It is important to point out that when modeling the evolution of the modes in the cavity, one encounters the challenge of enforcing correct initial conditions on the electromagnetic field (see Appendix 2 for details).

PROCEDURE AND RESULTS

Three teaching modules are provided, along with the associated MATLAB codes. Table 1 lists the name of each module along with the relevant input/output parameters and learning objectives. Teaching Module 1 introduces a student to electromagnetic waves and illustrates the difference between propagating EM waves and cavity modes. Teaching Module 2 illustrates the changes as the number of modes in the cavity increases. Here a clear demonstration of the transition from the standing wave (single mode) to the propagating pulse

(multiple modes) can be visualized. Teaching Module 3 illustrates the effect of mode locking on the laser output. It clearly shows that mode locking is a necessary condition for pulsed output and that the pulse intensity and width depend on the number of coherent modes. It also shows how the spacing between pulses changes with the length of the cavity. Appendix 3 provides more information about each module.

CLASS EXPERIENCE AND CONCLUSIONS

These teaching modules can be targeted toward both graduate and undergraduate physical chemistry students. The key advantage of the modules presented here is that the student can visualize the outcome without strong mathematical skills. A short introduction to MATLAB may need to be provided, possibly by a teaching assistant during the recitation session. However, an in-depth knowledge of coding in MATLAB is not needed since the codes for the three Teaching Modules are already provided here. The students would simply need to be instructed to the line of the code where parameters need to be changed.

The modules described here were introduced to 15 physical chemistry Ph.D. students at the University of Illinois Chicago as part of the Special Topics in Physical Chemistry course. The lecture material on cavity modes was presented in a sequence of three 1 hour lectures that introduced motivational examples illustrating the significance of ultrafast lasers in scientific

research, provided theoretical background on cavity modes and mode locking, and described codes written for our teaching modules on mode locking. The third lecture involved a hands-on experience where students worked with the codes described in Teaching Modules 1–3. Students were asked to change input parameters, visualize the outcome, and discuss whether the observed outcome made sense. After these three lectures, students were asked to evaluate their experience. Their responses were quite positive: they particularly appreciated the visual aspect provided by the graphs and animated videos, which helped them develop good intuition on how different parameters affect cavity modes. We anticipate that these teaching tools will be very useful to chemistry students at many levels, giving them an intuition for electromagnetic waves and lasers.

■ ASSOCIATED CONTENT

SI Supporting Information

The Supporting Information is available at <https://pubs.acs.org/doi/10.1021/acs.jchemed.2c00981>.

MATLAB file for Teaching Module 3 (TXT)

MATLAB file for Teaching Module 1 (TXT)

MATLAB file for Teaching Module 2 (TXT)

Video for Teaching Module 1a (MOV)

Video for Teaching Module 1b (MOV)

Video for Teaching Module 2a (MOV)

Video for Teaching Module 2b (MOV)

Video for Teaching Module 2c (MOV)

Appendices and Figures TM3a and TM3b associated with Teaching Module 3 (PDF)

■ AUTHOR INFORMATION

Corresponding Author

Ksenija D. Glusac – Department of Chemistry, University of Illinois Chicago, Chicago, Illinois 60607, United States; Chemical Sciences and Engineering, Argonne National Laboratory, Lemont, Illinois 60439, United States; orcid.org/0000-0002-2734-057X; Email: glusac@uic.edu

Author

Alexei Goun – Department of Chemistry, Princeton University, Princeton, New Jersey 08544, United States

Complete contact information is available at: <https://pubs.acs.org/10.1021/acs.jchemed.2c00981>

Notes

The authors declare no competing financial interest.

■ ACKNOWLEDGMENTS

K.D.G. thanks the National Science Foundation (1954298) for support.

■ REFERENCES

- (1) (a) Goun, A.; Glusac, K.; Fayer, M. Photoinduced Electron Transfer and Geminate Recombination in Liquids on Short Time Scales: Experiments and Theory. *J. Chem. Phys.* **2006**, *124* (8), 084504. (b) Singh, V.; Zoric, M. R.; Hargenrader, G. N.; Valentine, A. J.; Zivojinovic, O.; Milic, D. R.; Li, X.; Glusac, K. D. Exciton Coherence Length and Dynamics in Graphene Quantum Dot Assemblies. *J. Phys. Chem. Lett.* **2020**, *11* (1), 210–216. (c) Glusac, K.; Goun, A.; Fayer, M. Photoinduced Electron Transfer and Geminate Recombination in the Group Head Region of Micelles. *J. Chem. Phys.* **2006**, *125* (5), 054712. (d) Maiuri, M.; Garavelli, M.; Cerullo, G. Ultrafast Spectroscopy: State of the Art and Open Challenges. *J. Am. Chem. Soc.* **2020**, *142* (1), 3–15. (e) Li, G.; Glusac, K. D. The Role of Adenine in Fast Excited-state Deactivation of FAD: a Femtosecond Mid-IR Transient Absorption Study. *J. Phys. Chem. B* **2009**, *113* (27), 9059–9061. (f) Ilic, S.; Brown, E. S.; Xie, Y.; Maldonado, S.; Glusac, K. D. Sensitization of p-GaP with Monocationic Dyes: The Effect of Dye Excited-state Lifetime on Hole Injection Efficiencies. *J. Phys. Chem. C* **2016**, *120* (6), 3145–3155. (g) Oliver, T. A. Recent Advances in Multidimensional Ultrafast Spectroscopy. *R. Soc. Open Sci.* **2018**, *5* (1), 171425.
- (2) Polli, D.; Altoe, P.; Weingart, O.; Spillane, K. M.; Manzoni, C.; Brida, D.; Tomasello, G.; Orlandi, G.; Kukura, P.; Mathies, R. A.; Garavelli, M.; Cerullo, G. Conical Intersection Dynamics of the Primary Photoisomerization Event in Vision. *Nature* **2010**, *467* (7314), 440–443.
- (3) Johnson, P. J.; Halpin, A.; Morizumi, T.; Prokhorenko, V. I.; Ernst, O. P.; Miller, R. D. Local Vibrational Coherences Drive the Primary Photochemistry of Vision. *Nat. Chem.* **2015**, *7* (12), 980–986.
- (4) Li, G.; Parimal, K.; Vyas, S.; Hadad, C. M.; Flood, A. H.; Glusac, K. D. Pinpointing the Extent of Electronic Delocalization in the Re(I)-to-tetrazine Charge-separated Excited State using Time-resolved Infrared Spectroscopy. *J. Am. Chem. Soc.* **2009**, *131* (33), 11656–11657.
- (5) (a) Shaw, G. B.; Grant, C. D.; Shiota, H.; Castner, E. W.; Meyer, G. J.; Chen, L. X. Ultrafast Structural Rearrangements in the MLCT Excited State for Copper(I) Bis-phenanthrolines in Solution. *J. Am. Chem. Soc.* **2007**, *129* (7), 2147–2160. (b) Cordones, A. A.; Lee, J. H.; Hong, K.; Cho, H.; Garg, K.; Boggio-Pasqua, M.; Rack, J. J.; Huse, N.; Schoenlein, R. W.; Kim, T. K. Transient Metal-centered States Mediate Isomerization of a Photochromic Ruthenium-sulfoxide Complex. *Nat. Commun.* **2018**, *9* (1), 1989. (c) Chen, L. X.; Zhang, X.; Shelby, M. Recent Advances on Ultrafast X-ray Spectroscopy in the Chemical Sciences. *Chem. Sci.* **2014**, *5* (11), 4136–4152.
- (6) Ranitovic, P.; Hogle, C. W.; Rivière, P.; Palacios, A.; Tong, X.-M.; Toshima, N.; González-Castrillo, A.; Martin, L.; Martín, F.; Murnane, M. M.; Kapteyn, H. Attosecond Vacuum UV Coherent Control of Molecular Dynamics. *Proc. Natl. Acad. Sci. U. S. A.* **2014**, *111* (3), 912–917. Dantus, M.; Lozovoy, V. V. Experimental Coherent Laser Control of Physicochemical Processes. *Chem. Rev.* **2004**, *104* (4), 1813–1860.
- (7) Helmchen, F.; Denk, W. Deep Tissue Two-photon Microscopy. *Nat. Methods* **2005**, *2* (12), 932–940.
- (8) Camp, C. H., Jr.; Cicerone, M. T. Chemically Sensitive Bioimaging with Coherent Raman Scattering. *Nat. Photonics* **2015**, *9* (5), 295–305.
- (9) Malinauskas, M.; Farsari, M.; Piskarskas, A.; Juodkasis, S. Ultrafast Laser Nanostructuring of Photopolymers: A Decade of Advances. *Phys. Rep.* **2013**, *533* (1), 1–31.
- (10) Armstrong, M. R.; Zaug, J. M.; Goldman, N.; Kuo, I.-F. W.; Crowhurst, J. C.; Howard, W. M.; Carter, J. A.; Kashgarian, M.; Chesser, J. M.; Barbee, T. W.; Bastea, S. Ultrafast Shock Initiation of Exothermic Chemistry in Hydrogen Peroxide. *J. Phys. Chem. A* **2013**, *117* (49), 13051–13058.
- (11) Kimel, A. V.; Kirilyuk, A.; Rasing, T. Femtosecond Optomagnetism: Ultrafast Laser Manipulation of Magnetic Materials. *Laser Photonics Rev.* **2007**, *1* (3), 275–287.
- (12) Weiner, A. M. *Ultrafast Optics*; John Wiley & Sons, 2009.
- (13) Picqué, N.; Hänsch, T. W. Frequency Comb Spectroscopy. *Nat. Photonics* **2019**, *13* (3), 146–157.
- (14) (a) McHale, J. L. *Molecular Spectroscopy*; CRC Press, 2017. Battacharyya, A. *Ultrafast Optics and Spectroscopy in Physical Chemistry*; World Scientific, 2018. (b) Struve, W. S. *Fundamentals of Molecular Spectroscopy*; John Wiley & Sons, 1989. (c) Kelley, A. M. *Condensed-Phase Molecular Spectroscopy and Photophysics*; John Wiley & Sons, 2013. Siegman, A. E. *Lasers*; University Science Books, 1986.

- (15) Demtroder, W. *Laser Spectroscopy*; Springer, 2014. Abramczyk, H. *Introduction to Laser Spectroscopy*; Elsevier Science, 2005.
- (16) MATLAB; The Math Works: Natick, MA, 2021.
- (17) (a) Zoerb, M. C.; Harris, C. B. A simulation program for dynamic infrared (IR) spectra. *J. Chem. Educ.* **2013**, *90* (4), 506–507. (b) Joss, L.; Müller, E. A. Machine Learning for Fluid Property Correlations: Classroom Examples with MATLAB. *J. Chem. Educ.* **2019**, *96* (4), 697–703. (c) Fisher, A. A. An Introduction to Coding with MATLAB: Simulation of X-ray Photoelectron Spectroscopy by Employing Slater's Rules. *J. Chem. Educ.* **2019**, *96* (7), 1502–1505. (d) Li, X.; Huang, Z. J. An Inverted Classroom Approach to Educate MATLAB in Chemical Process Control. *Educ Chem. Eng.* **2017**, *19*, 1–12. (e) Stephens, L. I.; Mauzeroll, J. Demystifying Mathematical Modeling of Electrochemical Systems. *J. Chem. Educ.* **2019**, *96* (10), 2217–2224. (f) Fernández-Terán, R. J.; Sucre-Rosales, E.; Echevarria, L.; Hernández, F. E. A Sweet Introduction to the Mathematical Analysis of Time-Resolved Spectra and Complex Kinetic Mechanisms: The Chameleon Reaction Revisited. *J. Chem. Educ.* **2022**, *99* (6), 2327–2337. (g) Fisher, A. A. Developing the Chemist's Inner Coder: A MATLAB Tutorial on the Stochastic Simulation of a Pseudo-First-Order Reaction. *J. Chem. Educ.* **2020**, *97* (5), 1476–1480.
- (18) The MathWorks. *MATLAB Compiler SDK*. <https://www.mathworks.com/products/matlab-compiler-sdk.html> (accessed 2022-10-03).